Heliyon 10 (2024) e23448

Contents lists available at ScienceDirect

Heliyon

journal homepage: www.cell.com/heliyon

The value of contrast-enhanced magnetic resonance imaging for diagnosis of extrahepatic cholangiocarcinoma

Ting Yang [a,#], Hong Wei [a,#], Jie Chen [a,#], Hanyu Jiang [a], Yidi Chen [a,**,1], Bin Song [a,b,*,1]

[a] Department of Radiology, West China Hospital, Sichuan University, Chengdu, China
[b] Department of Radiology, Sanya People's Hospital, Sanya, Hainan, China

ARTICLE INFO

Keywords:
Cholangiocarcinoma
Diagnosis
Magnetic resonance imaging

ABSTRACT

Rationale and objectives: To establish a diagnostic model based on contrast-enhanced magnetic resonance imaging (MRI) and clinical characteristics for diagnosing extrahepatic cholangiocarcinoma (eCCA).

Materials and methods: From April 2014 to September 2021, consecutive patients with extrahepatic bile duct lesions who underwent contrast-enhanced MRI within 1 month before pathological examination were retrospectively enrolled. Two radiologists blinded to clinicopathological information independently evaluated MR images. Univariable and multivariable logistic regression analyses were performed to identify significant clinicoradiological features associated with eCCA, which were subsequently incorporated into a diagnostic model. Model performance was assessed using the area under the receiver operating characteristic curve (AUC), calibration curve, and decision curve.

Results: A total of 182 patients (mean age, 60.8 ± 10.0 years, 117 men) were included, 144 (79 %) of whom had pathologically confirmed eCCA. Diffusion restriction (odds ratio [OR], 8.32; 95 % confidence interval [CI]: 2.88, 25.82; $P < 0.001$), indistinct outer margin (OR, 4.01; 95 % CI: 1.40, 11.84; $P = 0.010$), cholelithiasis (OR, 0.34; 95 % CI: 0.12, 1.00; $P = 0.049$), serum ln (carbohydrate antigen 125) (OR, 4.95; 95 % CI: 1.61, 18.55; $P = 0.010$), and serum ln(direct bilirubin) (OR, 1.82; 95 % CI: 1.29, 2.63; $P < 0.001$) were independently associated with eCCA. Incorporating the above 5 variables, a diagnostic model achieved an AUC of 0.912 (95 % CI: 0.859, 0.965), with well-fitted calibration curve ($P = 0.815$) and good clinical utility. Additionally, the sensitivity, specificity and accuracy of the model were 83.33 %, 86.84 %, and 84.07 %, respectively.

Conclusion: The proposed model integrating two MRI features (i.e., indistinct outer margin and diffusion restriction) and three clinical characteristics (i.e., cholelithiasis, lnCA125 and lnDBIL) enabled accurate diagnosis of eCCA. This tool holds the potential to facilitate an early diagnosis and thereby allow timely treatment interventions and improved clinical outcomes for patients with eCCA.

* Corresponding author. Department of Radiology, West China Hospital, Sichuan University, No. 37 Guoxue Alley, Chengdu 610041, China.
** Corresponding author.
E-mail addresses: 992258245@qq.com (T. Yang), Weih_cat@163.com (H. Wei), jiechen_radi@foxmail.com (J. Chen), hanyu_jiang@foxmail.com (H. Jiang), chenyidi1152@126.com (Y. Chen), songlab_radiology@163.com (B. Song).
[#] These authors contributed equally to this work.
[1] These authors are co-corresponding authors.

https://doi.org/10.1016/j.heliyon.2023.e23448
Received 25 October 2023; Received in revised form 1 December 2023; Accepted 4 December 2023
Available online 10 December 2023

Introduction

Extrahepatic cholangiocarcinoma (eCCA) is the most prevalent type of biliary tract malignancy worldwide, encompassing two subtypes: perihilar cholangiocarcinoma (50–60 % of cases) and distal cholangiocarcinoma (20–30 % of cases) [1,2]. Surgical resection stands as the primary curative treatment for eCCA [3,4]. However, the preoperative diagnosis of eCCA is challenging, as early-stage eCCA often presents with subtle symptoms and atypical clinical manifestations. Additionally, substantial overlaps in clinical and imaging features exist between eCCA and other benign (e.g., cholangiolithiasis, cholangitis) and malignant (e.g., pancreatic head cancer) entities. Furthermore, the technical difficulty in obtaining biopsies through endoscopic retrograde cholangiopancreatography for lesions located distant from the duodenal ampulla further complicates the matters. In these contexts, clinicians sometimes opt for a "wait-and-see" protocol, potentially resulting in the loss of opportunities for surgical intervention. Therefore, the identification of accurate and reliable diagnostic markers for eCCA is of paramount importance to facilitate timely treatment and enhance patient outcomes.

To date, contrast-enhanced magnetic resonance imaging (MRI) is widely regarded as the most accurate noninvasive technique for diagnosing eCCA [5]. It offers a comprehensive assessment of tumor morphology, hemodynamics, as well as biliary duct anatomy, macrovascular invasion, regional lymph node, and distant metastases. Previous studies have demonstrated that several MRI features, such as diffusion restriction, irregular tumor margins, asymmetric biliary strictures, wall thickening, long segment involvement, and hypovascularity with gradual enhancement could be used to diagnose eCCA with accuracies ranging from 72.00 % to 94.20 % [6–13].

Despite promising results, the high prevalence of immunoglobulin G4 (IgG4)-related sclerosing cholangitis in Asia brought challenges to differentiate it from eCCA due to several overlapping characteristics [14]. Both conditions can present with biliary strictures, dilatation of the bile ducts, and wall thickening, making it challengeable to establish a definitive diagnosis through imaging [15]. Thus, a combination of clinical, serological, and radiological findings is necessary to diagnose eCCA. Currently, few studies have been conducted to develop noninvasive diagnostic models for eCCA based on MRI and clinical features. Meanwhile, these studies had relatively small sample size (e.g., 42–78 patients) and reported inconsistent findings [6–13].

Therefore, the purpose of our study was to develop a noninvasive diagnostic model for eCCA based on contrast-enhanced MRI and clinical characteristics.

Materials and Methods

This single-center retrospective study was was conducted in accordance with the principles of the World Medical Association Declaration of Helsinki and was approved by the Biomedical Ethics Review Committee of West China Hospital, Sichuan University (Approval Number: 2021-107), and the requirements for written informed consent were waived.

Patients

Between April 2014 and September 2021, consecutive patients were enrolled according to the following inclusion criteria: (a) age $\geq$18 years; (b) with pathologically-proven extrahepatic bile duct lesions; and (c) underwent contrast-enhanced MRI within 1 month before pathological examination. Exclusion criteria were: (a) patients with any prior or current malignancies other than eCCA; (b) suboptimal MR imaging quality (e.g., severe artifact); and (c) incomplete clinical or pathological data.

Baseline clinical data were recorded as follows: (a) patient demographics; (b) presence or absence of choledochal cyst, cholelithiasis, cirrhosis, and obstructive jaundice according to clinical diagnosis; (c) serum levels of carcinoembryonic antigen (CEA), carbohydrate antigen 19-9 (CA19-9), carbohydrate antigen 125 (CA125), total bilirubin (TBIL), direct bilirubin (DBIL), aspartate aminotransferase (AST), alanine aminotransferase (ALT), alkaline phosphatase (ALP), gamma-glutamyl transferase (GGT), albumin (ALB), total cholesterol (TC); and (d) Child-Pugh stage.

Image acquisition

MRI was performed with various 1.5 T or 3.0 T systems. The baseline contrast-enhanced MRI examination include (a) T2-weighted imaging (T2WI); (b) magnetic resonance cholangiopancreatography; (c) diffusion-weighted imaging (DWI) (b values: 0, 50, 500, 800, 1000, and 1200 s/mm2 [Siemens MAGNETOM Skyra]; 0, 50, 1000 s/mm2 [uMR588]; 0, 50, 800, 1000 s/mm2 [Siemens Avanto]; 0, 50, 600 s/mm2 [Siemens TrioTim]) with apparent diffusion coefficient (ADC) maps reconstructed by monoexponential model. (d) T1-weighted in-phase and opposed-phase imaging; (e) dynamic T1-weighted imaging (T1WI) before and after injection of contrast agent in the arterial phase (AP), portal venous phase (PVP), transitional phase (TP) (for hepatobiliary contrast agent) or the delayed phase (DP) (for extracellular contrast agent). Imaging protocols are detailed in **Supplementary A1 an d Table S1.**

Image analysis

All de-identified MR images were independently reviewed by two radiologists (with 3 and 10 years of experience in abdominal MRI, respectively) who were blinded to clinical and pathological information. Any disagreements between the two readers were resolved through discussions.

For each patient, the following imaging features were assessed: (a) longest diameter of the lesion; (b) presence or absence of

imaging features related to disease diagnosis (e.g., wall thickness, segment involvement, indistinct outer margin, enhancement pattern, diffusion restriction and severe bile duct dilatation) [7,16,17]; and (c) other imaging features of interest (e.g., growth pattern, adjacent organ involvement, macrovascular invasion, lymph node metastasis) [18]. The definitions for all assessed imaging features can be found in Table S2.

Reference standard

Histopathological information was retrieved from routine reports to serve as the reference standard for diagnosing extrahepatic bile duct diseases. Following institutional standard practice procedure, two experienced pathologists independently evaluated the histopathological types of lesions according to the fifth edition of the digestive system tumor classification standard issued by the World Health Organization [19]. Any discrepancies between the two pathologists were resolved through either mutual consultation or involvement of a third senior pathologist.

Statistical analysis

Continuous variables were presented as mean ± standard deviation or median (interquartile range [IQR]) and compared using the Student's *t*-test or Mann-Whitney *U* test, whereas categorical variables were presented as the numbers of cases (percentages) and compared with the chi-square test or the Fisher's exact test, as appropriate.

To evaluate interobserver agreement in MRI interpretation, intraclass correlation coefficient (ICC), Cohen's κ coefficient and weighted κ coefficient were calculated for continuous variables, binary variables, and categorical variables, respectively.

Development of the predictive model for eCCA

To improve the clinical utility, the continuous variables were transformed into both natural logarithm and categorical form according to the normal ranges or clinical relevance. Univariable and multivariable logistic regression analyses were used to identify predictors of eCCA while controlling for age and gender. Variables with $P < 0.05$ in the univariable analysis were subsequently included in the multivariable logistic regression model using five-fold cross-validation. Spearman's correlation analysis was performed to assess intervariable collinearity. In cases where there were correlated variables (Spearman correlation coefficient >0.6), only the variable with the largest odds ratio (OR) from the univariable analysis was retained for further analysis. The final model was selected by backward stepwise elimination with Akaike information criteria.

Assessment of the model performance

The discrimination performance of the model was quantified by the area under the receiver operating characteristic curve (AUC), and the optimal threshold was determined with the Youden's index. Model fitness was assessed by a calibration curve with the Hosmer-Lemeshow test. The clinical utility of the model was evaluated by decision curve analysis. Additionally, sensitivity, specificity, positive predictive value (PPV), negative predictive value (NPV), and accuracy were computed.

All statistical analyses were performed with R software (version 4.2.2; R Foundation for Statistical Computing) or Medcalc (version 20.112; MedCalc Software). Two-tailed $P < 0.05$ was considered statistically significant.

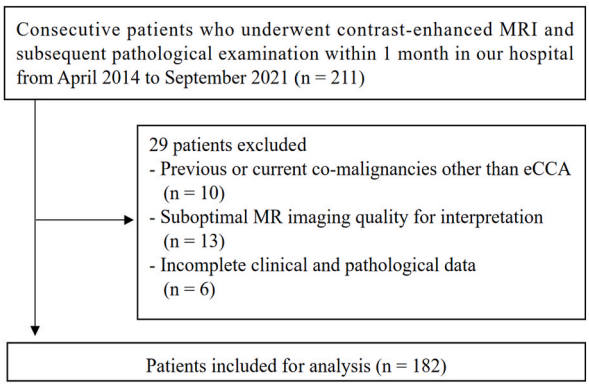

Fig. 1. Flowchart of patient selection. MRI = magnetic resonance imaging.

Table 1
Comparison of baseline clinical characteristics of non-eCCA patients and eCCA patients.

Characteristics	All (n = 182)	eCCA (n = 144)	Non-eCCA (n = 38)	*P* value
Age (y)[a]	60.8 ± 10.0	60.8 ± 10.0	56.2 ± 14.5	0.004
Sex				0.047
Male	117 (64.3)	92 (63.9)	25 (34.2)	
Female	65 (35.7)	52 (36.1)	13 (65.8)	
Risk factor				
Choledochal cyst	3 (1.6)	0 (0.0)	3 (7.9)	0.009
Cholelithiasis	39 (21.4)	23 (16.0)	16 (42.1)	<0.001
Liver cirrhosis	8 (4.4)	4 (2.8)	4 (10.5)	0.104
Obstructive jaundice	91 (50.0)	79 (54.9)	12 (31.6)	0.011
Laboratory index				
CEA (ng/ml)				0.005
≤5	149 (81.9)	112 (77.8)	37 (97.4)	
>5	33 (18.1)	32 (22.2)	1 (2.6)	
CA199 (U/ml)				<0.001
≤100	90 (49.5)	59 (41.0)	31 (81.6)	
>100	92 (50.5)	85 (59.0)	7 (18.4)	
CA125 (continues) (U/ml)[b]	20.6 (15.1, 30.0)	20.6 (15.1, 29.7)	14.9 (10.5, 18.9)	<0.001
lnCA125[b]	3.0 (2.7, 3.4)	3.0 (2.7, 3.4)	2.7 (2.3, 2.9)	<0.001
CA125 (category) (U/ml)				0.003
≤35	154 (84.6)	116 (80.6)	38 (100.0)	
>35	28 (15.4)	28 (19.4)	0 (0.0)	
TBIL (continues) (μmol/L)[b]	141.5 (64.9, 230.1)	141.5 (65.6, 229.4)	17.4 (11.0, 104.3)	<0.001
lnTBIL[b]	5.0 (4.2, 5.4)	5.0 (4.2, 5.4)	2.8 (2.4, 4.6)	<0.001
TBIL (category) (μmol/L)				<0.001
≤28	38 (20.9)	16 (11.1)	22 (57.9)	
>28	144 (79.1)	128 (88.9)	16 (42.1)	
DBIL (continues) (μmol/L)[b]	121.9 (57.4, 201.5)	121.9 (57.6, 200.3)	11.2 (4.1, 88.8)	<0.001
lnDBIL[b]	4.8 (4.0, 5.3)	4.8 (4.1, 5.3)	2.4 (1.4, 4.5)	<0.001
DBIL (category) (μmol/L)				<0.001
≤8.8	29 (15.9)	11 (7.6)	18 (47.4)	
>8.8	153 (84.1)	133 (92.4)	20 (52.6)	
AST (continues) (IU/L)[b]	76.5 (54.5, 120.5)	76.5 (54.8, 120.3)	37 (24.3, 101.5)	<0.001
lnAST[b]	4.3 (4.0, 4.8)	4.3 (4.0, 4.8)	3.6 (3.2, 4.6)	<0.001
AST (category) (IU/L)				<0.001
≤35	30 (16.5)	15 (10.4)	15 (39.5)	
>35	152 (83.5)	129 (89.6)	23 (60.5)	
ALT (continues) (IU/L)[b]	95.5 (59.0, 159.0)	95.5 (59.0, 158.5)	44.5 (32.0, 139.0)	0.004
lnALT[a]	4.6 ± 0.8	4.6 ± 0.8	4.1 ± 1.0	0.015
ALT (category) (IU/L)				<0.001
≤40	37 (20.3)	20 (13.9)	17 (44.7)	
>40	145 (79.7)	124 (86.1)	21 (55.3)	
ALP (continues) (IU/L)[b]	358.5 (213.0, 603.5)	358.5 (213.5, 601.8)	197.5 (123.0, 359.8)	<0.001
lnALP[a]	5.9 ± 0.7	5.9 ± 0.7	5.4 ± 0.8	0.159
ALP (category) (IU/L)				<0.001
≤160	36 (19.8)	21 (14.6)	15 (39.5)	
>160	146 (80.2)	123 (85.4)	23 (60.5)	
GGT (continues) (IU/L)[b]	384.0 (173.0, 932.0)	384.0 (173.0, 930.5)	256.0 (109.5, 551.8)	0.029
lnGGT[a]	5.9 ± 1.1	5.9 ± 1.1	5.4 ± 1.4	0.137
GGT (category) (IU/L)				0.064
≤60	17 (9.3)	10 (6.9)	7 (18.4)	
>60	165 (90.7)	134 (93.1)	31 (81.6)	
TC (continues) (μmol/L)[b]	5.2 (4.3, 7.1)	5.2 (4.3, 7.1)	4.8 (3.8, 5.6)	0.016
lnTC[b]	1.7 (1.5, 2.0)	1.7 (1.5, 2.0)	1.6 (1.3, 1.7)	0.016
TC (category) (μmol/L)				0.008
≤5.7	115 (63.2)	84 (58.3)	31 (81.6)	
>5.7	67 (36.8)	60 (41.7)	7 (18.4)	
ALB (continues) (g/L)[a]	38.5 ± 4.8	38.5 ± 4.8	40.2 ± 4.3	0.555
lnALB[a]	3.6 ± 0.1	3.6 ± 0.1	3.7 ± 0.1	0.841
ALB (category) (g/L)				0.386
>40	75(41.2)	57 (39.6)	18 (47.4)	
≤40	107(58.8)	87 (60.4)	20 (52.6)	
Child-Pugh stage				<0.001

(*continued on next page*)

Table 1 (*continued*)

Characteristics	All (n = 182)	eCCA (n = 144)	Non-eCCA (n = 38)	*P* value
A	52 (28.6)	26 (18.1)	26 (68.4)	
B	130 (71.4)	118 (81.9)	12 (31.6)	
C	0 (0.0)	0 (0.0)	0 (0.0)	

Note.—Data are expressed as n (%) or median (interquartile range). eCCA = extrahepatic cholangiocarcinoma, CEA = carcinoembryonic antigen, CA199 = carbohydrate antigen 199, CA125 = carbohydrate antigen 125, TBIL = total bilirubin, DBIL = direct bilirubin, AST = aspartate aminotransferase, ALT = alanine aminotransferase, ALP = alkaline phosphatase, GGT = gamma-glutamyl transferase, ALB = albumin, TC = total cholesterol.

Continuous variables are presented as mean ± standard deviation. Categorical variables are the number of patients, with percentages in parentheses.

[a] Continuous variables that conform to the normal distribution were expressed as mean ± standard deviation.

[b] Continuous variables with non-normal distribution expressed as median (interquartile range).

Results

Patient characteristics

A total of 182 patients (mean age, 60.8 ± 10.0 years; 117 men) were included (Fig. 1), among whom 79.1 % (144/182) had pathologically confirmed eCCA and 20.9 % (38/182) were diagnosed with benign lesions, including chronic cholangitis (15.9 %, 29/182), biliary papilloma (3.8 %, 7/182), biliary tuberculosis (0.5 %, 1/182), and traumatic neuroma (0.5 %, 1/182). Baseline clinical characteristics are shown in Table 1, and frequencies of MRI features are summarized in Table 2. Interobserver agreement of MRI features is presented.

in Table S3.

Regarding clinical characteristics, eCCA was more frequently observed in old, male patients with less frequent choledochal cyst (P = 0.009) and cholelithiasis (P < 0.001), more frequent obstructive jaundice (P = 0.011), and more advanced Child-Pugh stage (P < 0.001). In terms of laboratory indices, patients with eCCA had elevated serum levels of CEA (*P* = 0.005), CA199 (*P* < 0.001), CA125 (*P*

Table 2
Frequencies of contrast-enhanced MRI features.

MRI features	All (n = 182)	eCCA (n = 144)	Non-eCCA (n = 38)	*P* value
Location				0.002
Perihilar	120 (65.9)	103 (71.5)	17 (44.7)	
Distal	62 (34.1)	41 (28.5)	21 (55.3)	
Growth pattern				0.005
Mass-forming	27 (14.8)	26 (18.1)	1 (2.6)	
Periductal infiltrating	97 (53.3)	76 (52.8)	21 (55.3)	
Intraductal growing	47 (25.8)	31 (21.5)	16 (42.1)	
Mixed	11 (6.0)	11 (7.6)	0 (0.0)	
Lesion size (mm)*	27.0 (20.0–36.0)	27.0 (22.0–34.0)	24.0 (17.0–46.0)	0.259
Wall thickness (mm)*	5.5 (4.0–8.0)	6.0 (4.0–8.0)	4.0 (3.0–7.0)	0.023
Segment involvement (mm)*	31.0 (22.0–41.0)	29.0 (24.0–38.0)	41.0 (17.0–53.0)	0.422
Indistinct outer margin	146 (80.2)	125 (86.8)	21 (55.3)	<0.001
Asymmetric narrowing	160 (87.9)	131 (91.0)	29 (76.3)	0.029
Abrupt narrowing	155 (85.2)	131 (91.0)	24 (63.2)	<0.001
Pre-contrast T2WI mild hyperintensity	83 (45.6)	64 (44.4)	19 (50.0)	0.541
Pre-contrast T1WI mild hyperintensity	88 (48.4)	76 (52.8)	12 (31.6)	0.020
Hyperenhancing in the AP	85 (46.7)	70 (48.6)	15 (39.5)	0.315
Hyperenhancing in the PVP	134 (73.6)	115 (79.9)	19 (50.0)	<0.001
Hyperenhancing in the TP or DP	143 (78.6)	119 (82.6)	24 (63.2)	0.009
Enhancement pattern				0.044
Similar to that of the uninvolved bile duct	19 (10.4)	11 (7.6)	8 (21.1)	
Hypovascularity with gradual enhancement	94 (51.6)	75 (52.1)	19 (50.0)	
Hypervascularity on arterial or portal venous phase images with persistent or washout enhancement	69 (37.9)	58 (40.3)	11 (28.9)	
Diffusion restriction	148 (81.3)	130 (90.3)	18 (47.4)	<0.001
Severe dilation of the intrahepatic bile duct	82 (45.1)	66 (45.8)	16 (42.8)	0.681
Invasion of the adjacent organ	62 (34.1)	57 (39.6)	5 (13.2)	0.002
Macrovascular invasion	76 (41.8)	71 (49.3)	5 (13.2)	<0.001
Lymph node metastasis	47 (25.8)	40 (27.8)	7 (18.4)	0.241

Note.—Data are expressed as the frequencies of MRI features, with percentages in parentheses. MRI = magnetic resonance imaging, T1WI = T1 weighted imaging, T2WI = T2 weighted imaging, AP = arterial phase, PVP = portal venous phase, TP = transitional phase, DP = delayed phase.

< 0.001), TBIL ($P < 0.001$), DBIL ($P < 0.001$), AST ($P < 0.001$), ALT ($P = 0.004$), ALP ($P < 0.001$), GGT ($P = 0.029$), and TC ($P = 0.016$) in comparison to those without eCCA. There were no significant differences in other clinical characteristics between the eCCA and non-eCCA cohorts ($P = 0.064$–0.841).

As for radiologic features, eCCA was found to be more commonly located in the perihilar area ($P = 0.002$), demonstrating higher frequencies of mass-forming and mixed growth patterns ($P = 0.005$), and exhibiting a larger wall thickness ($P = 0.023$). Indistinct outer margin ($P < 0.001$), asymmetric narrowing ($P = 0.029$), abrupt narrowing ($P < 0.001$), pre-contrast T1WI mild hyperintensity ($P = 0.020$), hyperenhancement in the PVP ($P < 0.001$), hyperenhancement in the TP or DP ($P = 0.009$), hypovascularity with gradual enhancement and hypervascularity on arterial or portal venous phase images with persistent or washout enhancement patterns ($P = 0.044$), diffusion restriction ($P < 0.001$), invasion of the adjacent organ ($P = 0.002$), and macrovascular invasion ($P < 0.001$) were significantly more frequent in eCCAs compared to non-eCCAs. No statistically significant differences were observed in other radiologic features between the two groups ($P = 0.241$–0.681).

Development of the predictive model for eCCA

At univariable analysis, 7 clinicoradiological variables were significantly associated with eCCA, including cholelithiasis (odds ratio [OR], 0.23; 95 % confidence interval [CI]: 0.10, 0.52; $P < 0.001$), lnCA125 (OR, 7.05; 95 % CI: 2.72, 18.25; $P < 0.001$), lnDBIL (OR, 2.46; 95 % CI: 1.82, 3.33; $P < 0.001$), indistinct outer margin (OR, 5.80; 95 % CI: 2.53, 13.30; $P < 0.001$), T1WI hyperintensity (OR, 2.28; 95 % CI: 1.06, 4.90; $P = 0.036$), hyperenhancement in the PVP (OR, 3.97; 95 % CI: 1. 86, 8. 44; $P < 0.001$) and diffusion restriction(OR, 11.58; 95 % CI: 4.79, 28.01; $P < 0.001$) (Table S4). Multivariate analysis identified cholelithiasis (OR, 0.34; 95 % CI: 0.12, 1.00; $P = 0.049$), lnCA125 (OR, 4.95; 95 % CI: 1.61, 18.55; $P = 0.010$), lnDBIL (OR, 1.82; 95 % CI: 1.29, 2.63; $P < 0.001$), indistinct outer margin (OR, 4.01; 95 % CI: 1.40, 11.84; P = 0.010), and diffusion restriction (OR, 8.32; 95 % CI: 2.88, 25.82; $P < 0.001$) as independent predictors for eCCA (Table 3). Based on the variables mentioned above, a diagnostic model was developed and can be described by the following formula: Y = - 7.6624 - 1.0689 × cholelithiasis +1.5995 × lnCA125 + 0.5980 × lnDBIL +1.3888 × indistinct outer margin +2.1181 × diffusion restriction (Fig. 2).

Model performances

The diagnostic model for eCCA yielded an AUC of 0.912 (95 % CI: 0.859, 0.965) (Fig. 3A). The calibration plot demonstrated that the model-predicted probabilities were consistent with the actual eCCA cases ($P = 0.815$) (Fig. 3B). Moreover, decision curve analysis illustrated a greater net benefit of the model than assuming all patients had eCCA across the threshold ranges (Fig. 3C). Using a threshold of 0.805, the model achieved a sensitivity, specificity, PPV, NPV and accuracy of 83.33 % (95 % CI: 76.22 %, 89.02 %), 86.84 % (95 % CI: 71.91 %, 95.59 %), 96.00 % (95 % CI: 91.36 %, 98.20 %), 57.89 % (95 % CI: 48.32 %, 66.91 %) and 84.07 % (95 % CI: 77.92 %, 89.06 %), respectively (Table 4). Diagnostic performance of each predictor included in the model are presented in Table 4. In addition, diagnostic performance of the combination of two predictive MRI features (i.e., indistinct outer margin and diffusion restriction) is presented in Table S5. To further evaluate the potential influence of MRI field strengths on the diagnostic performance of diffusion restriction, a subgroup analysis was conducted between MRI at 3.0 T and 1.5 T. The subgroup of MRI at 1.5 T demonstrated a significantly higher PPV than that of MRI at 3.0 T (90.60 % vs 77.42 %; $P = 0.046$). No significant differences were observed in other parameters between MRI at 3.0 T and 1.5 T (Table S6). An example of typical radiological characteristics of eCCA is shown in Fig. 4.

Discussion

In the present study, we developed a clinicoradiological model for noninvasive diagnosis of eCCA. By integrating two contrast-enhanced MRI features (indistinct outer margin and diffusion restriction) and three clinical characteristics (cholelithiasis, lnCA125

Table 3
Univariable and multivariable logistic regression analysis of predictors for eCCA.

Characteristics	Univariable analysis		Multivariable analysis		
	Odds ratio (95%CI)	*P* value	Odds ratio (95%CI)	β coefficient	*P* value
Cholelithiasis	0.23 (0.10,0.52)	<0.001	0.34 (0.12, 1.00)	−1.07	0.049
lnCA125	7.05 (2.72,18.25)	<0.001	4.95 (1.61, 18.55)	1.60	0.010
lnDBIL	2.46 (1.82,3.33)	<0.001	1.82 (1.29, 2.63)	0.60	<0.001
Indistinct outer margin	5.80 (2.53,13.30)	<0.001	4.01 (1.40, 11.84)	1.39	0.010
T1WI hyperintensity	2.28 (1.06,4.90)	0.036	…	…	…
Hyperenhancement in the PVP	3.97 (1.86,8.44)	<0.001	…	…	…
Diffusion restriction	11.58 (4.79,28.01)	<0.001	8.32 (2.88, 25.82)	2.12	<0.001

Note.—eCCA = extrahepatic cholangiocarcinoma, CI = confidence intervals, CA125 = carbohydrate antigen 125, DBIL = direct bilirubin, T1WI = T1 weighted imaging.
After removing variables with obvious collinearity (Spearman's rho >0.6) and variables which were not retained in the multivariable analysis that performed in the clinical parameter and radiologic feature, respectively, a total of 7 preoperative variables, including cholelithiasis, lnCA125, lnDBIL, indistinct outer margin, T1WI hyperintensity, hyperenhancement in the PVP and diffusion restriction, were analyzed in the multivariate logistic regression.

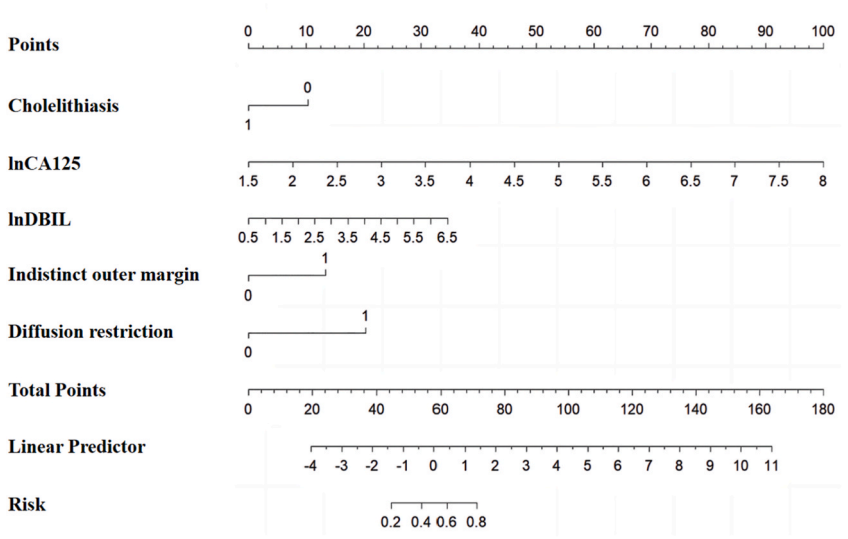

Fig. 2. Nomogram to predict the probability of extrahepatic cholangiocarcinoma. Predictor points of each variable are presented on point scale. CA125 = carbohydrate antigen 125, DBIL = direct bilirubin.

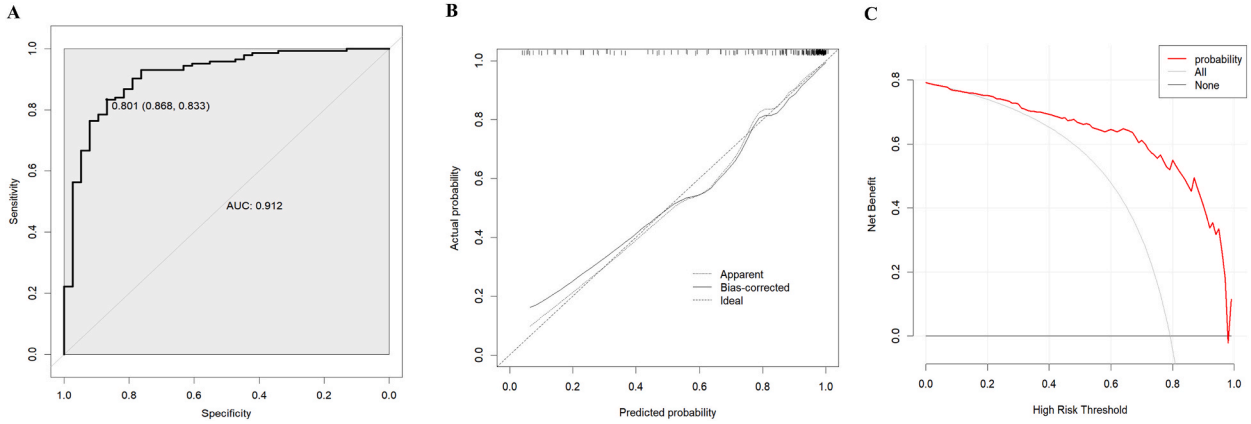

Fig. 3. (A) Area under the receiver operating characteristic curve, (B) calibration plot and (C) decision curve for predicting extrahepatic cholangiocarcinoma.

and lnDBIL), the model achieved good diagnostic performance and satisfactory calibration. Decision curve analysis further confirmed the clinical utility of the model.

A correlation was observed between eCCA and diffusion restriction in our study, which is consistent with previous studies [20–22]. It is well-known that diffusion restriction occurs when water molecule diffusions in the microenvironment of malignant tumor cells are hindered [23,24]. In a study conducted by Cui et al. involving 31 cases, DWI exhibited a sensitivity of 93.50 % for eCCA [21], which is similar to our study (sensitivity of 90.28 % for diffusion restriction). Additionally, Park et al. found that adding DWI to contrast-enhanced MRI could significantly improve the diagnostic accuracy of eCCA [7]. Based on these findings, we proposed that extrahepatic bile duct lesions demonstrating diffusion restriction were more likely to be classified as eCCAs.

Indistinct outer margin, defined as blurring, speculation, or irregularity of the outer margin of the involved bile duct wall, was another imaging predictor of eCCA in our study. This finding was in line with a study by Kim et al., which demonstrated that an indistinct outer margin was indicative of a malignant bile duct stricture with moderate sensitivity (76.20 %) and high specificity (91.30 %) [12]. This observation can be attributed to the inherent aggressive characteristics of eCCA [16].

In order to enhance the accuracy of the model, a comprehensive investigation was conducted on the diagnostic value of various forms of laboratory indices, including continuous, natural logarithm, and categorical variables. Our study found that the natural logarithm transformation of CA125 and DBIL were independent predictors associated with eCCA, as previously reported [25,26]. The exact mechanism underlying the association between CA125 and eCCA is not fully understood. However, it has been suggested that CA125 may play a role in tumor invasion and metastasis by promoting cell adhesion, migration, and angiogenesis [26]. Furthermore, biliary tract obstruction often leads to increased TBIL and DBIL levels, but our findings suggest that elevated DBIL may be more closely

Table 4
Diagnostic performance of five significant features and the model of their combinations for predicting eCCA.

Parameters	AUC (95 % CI)	Cut-off	Sensitivity (%) (95 % CI)	Specificity (%) (95 % CI)	PPV (%) (95 % CI)	NPV (%) (95 % CI)	ACC (%) (95 % CI)
Cholelithiasis	0.631 (0.556, 0.701)	…	84.03 (77.00, 89.60) [121/144]	42.11 (26.31, 59.18) [16/38]	84.62 (80.60, 87.92) [121/143]	41.03 (29.08, 54.13) [16/39]	75.28 (68.35,81.36) [137/182]
lnCA125	0.725 (0.654, 0.788)	>0.300	52.78 (44.29, 61.15) [76/144]	81.58 (65.67, 92.26) [31/38]	91.57 (84.53, 95.57) [76/83]	31.31 (26.60, 36.45) [31/99]	58.79 (51.27, 66.02) [107/182]
lnDBIL	0.798 (0.732, 0.854)	>0.395	85.42 (78.58, 90.74) [123/144]	71.05 (54.10, 84.58) [27/38]	91.79 (87.12, 94.87) [123/134]	56.25 (45.19, 66.72) [27/48]	82.42 (76.10, 87.65) [150/182]
Indistinct outer margin	0.658 (0.584, 0.726)	…	86.81 (80.16, 91.87) [125/144]	44.74 (28.62, 61.70) [17/38]	85.62 (81.62, 88.86) [125/146]	47.22 (34.09, 60.75) [17/36]	78.02 (71.30, 83.81) [142/182]
Diffusion restriction	0.715 (0.643, 0.779)	…	90.28 (84.223, 94.58) [130/144]	52.63 (35.82, 69.02) [20/38]	87.84 (83.72, 91.02) [130/148]	58.82 (44.39, 71.88) [20/34]	82.42 (76.10, 87.65) [150/182]
Model	0.912 (0.859, 0.965)	>0.805	83.33 (76.22, 89.02) [120/144]	86.84 (71.91, 95.59) [33/38]	96.00 (91.36, 98.20) [120/125]	57.89 (48.32, 66.91) [33/57]	84.07 (77.92, 89.06) [153/182]

Note.—Numbers in parentheses are 95 % confidence intervals, and numbers in brackets are raw data. eCCA = extrahepatic cholangiocarcinoma, CI = confidence intervals, CA125 = carbohydrate antigen 125, DBIL = direct bilirubin, AUC = area under the receiver operating characteristic curve, PPV = positive predictive value, NPV = negative predictive value, ACC = accuracy.

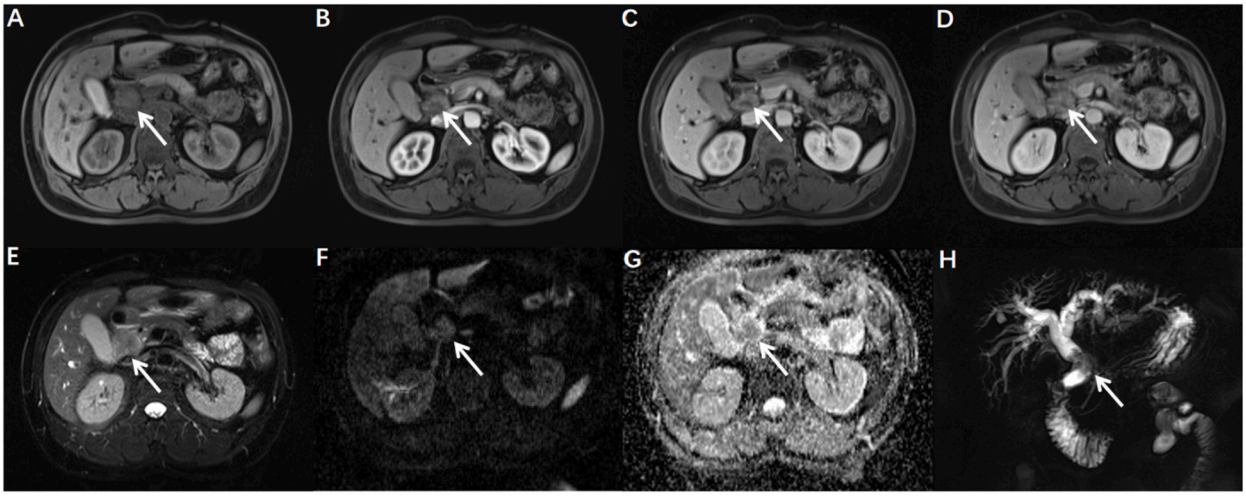

Fig. 4. Images in a 48-year-old man with pathologically-proven extrahepatic cholangiocarcinoma (white arrows).
(A) Pre-enhanced T1 weighted imaging shows a mild-hyperintensity lesion. The lesion presents mild hyperenhancement in the (B) arterial phase and it gradually peaks in the (C) portal venous phase and (D) transitional phase. (E) Axial T2 weighted imaging demonstrates an isointense tumor. Signal intensity of the lesion on (F) diffusion weighted imaging is unequivocally higher than the uninvolved bile duct wall, and that on (G) apparent diffusion coefficient map is unequivocally lower than the uninvolved bile duct wall. (F) Magnetic resonance cholangiopancreatography depicts filling defects with severely dilated bile ducts.

related to eCCA than DBIL. However, our results remain to be further validated in future large-scale studies.

Interestingly, our study found a negative association between cholelithiasis and eCCA when differentiating benign and malignant bile duct lesions, which contradicts prior research where cholelithiasis was a risk factor of eCCA [27–29]. This discrepancy might be explained in part by the different prevalence of cholelithiasis and cholangitis between the non-eCCA group and the eCCA group. Of note, cholelithiasis has been suggested a risk factor of both eCCA and cholangitis [30]. In our study, cholangitis was present in 76.3 % (29/38) of non-eCCA patients, while only 21.5 % (31/144) of eCCA patients had concurrent cholangitis. Consequently, in patients with cholelithiasis, 41.0 % (16/39) were cholangitis and only 10.3 % (4/39) were eCCA at pathology. Nowadays, evidence remains scarce regarding whether cholelithiasis is more associated with cholangitis or cholangiocarcinoma. Therefore, despite potential selection bias due to the limited number of pathologically confirmed non-eCCA patients, our findings implied a stronger relation between cholelithiasis and cholangitis when compared to eCCA. Nevertheless, a conclusive diagnosis should be reached by considering other imaging findings and tests. Future prospective, larger-scale, multicenter studies are needed to validate our findings.

Compared to prior studies with single-center retrospective design and limited number of patients (i.e., 42–78) [6–13], our study included a more substantial sample size, lending a greater validity to the results presented. Moreover, in the current study, the proposed model incorporating clinical, serological, and imaging findings showed superior accuracy for diagnosing eCCA compared to individual clinical or imaging feature examined both in this study and by previous studies [6–13]. This finding underscores the potential of the integrated model as a valuable diagnostic tool for eCCA.

Several limitations of our study should be noted. First, possible selection bias existed due to the unbalanced eCCA and non-eCCA sample sizes in this single-center retrospective study. Second, our sample size is limited because the morbidity of eCCA is low and contrast-enhanced MRI was not a routine diagnostic technique for eCCA from 2014 to 2016 in our hospital. Therefore, data partitioning and independent validation analysis were not performed in our study. Third, the interreader agreement of several imaging features were unsatisfactory because of the subjective interpretation. Further studies are warranted to develop an optimal strategy for reducing interreader variability in eCCA diagnosis. Finally, owing to the retrospective nature, different b-values were employed on multiple MRI scanners, which could potentially impact the performance of DWI in the identification of eCCA, as the contrast-to-noise ratio between the tumor and normal liver decreased when the b-value was increased from 100 s/mm^2 to 1000 s/mm^2 [31].

In conclusion, based on two contrast-enhanced MRI features (indistinct outer margin and diffusion restriction) and three clinical indicators (cholelithiasis, lnCA125 and lnDBIL), this work proposed an accurate diagnostic model for eCCA. Further validation is warranted to explore the generalizability of our model and facilitate its clinical translations.

Ethics statement

This study protocol was conducted in accordance with the principles of the World Medical Association Declaration of Helsinki and was approved by the Biomedical Ethics Review Committee of West China Hospital, Sichuan University (Approval Number: 2021-107). The requirement for informed consent was waived (retrospective design) by the Biomedical Ethics Review Committee of West China Hospital, Sichuan University. Participants consented to have their MR images published.

Funding

This study was funded by Science and Technology Support Program of Sichuan Province (Grant number 2022YFS0072), the 1.3.5 project for disciplines of excellence, West China Hospital, Sichuan University (Grant number ZYGD22004), Hainan Province Clinical Medical Center, and the Post-doctoral Station Development Project of Sanya.

Ethics approval

This study protocol was conducted in accordance with the principles of the World Medical Association Declaration of Helsinki and was approved by the Biomedical Ethics Review Committee of West China Hospital, Sichuan University (Approval Number: 2021-107). The requirement for informed consent was waived (retrospective design) by the Biomedical Ethics Review Committee of West China Hospital, Sichuan University. Participants consented to have their MR images published.

Consent for publication

Not required.

Funding statement

This study was funded by Science and Technology Support Program of Sichuan Province (Grant number 2022YFS0072), the 1.3.5 project for disciplines of excellence, West China Hospital, Sichuan University (Grant number ZYGD22004), Hainan Province Clinical Medical Center, and the Post-doctoral Station Development Project of Sanya.

Data availability statement

The data associated with our study has not been deposited into a publicly available repository.

Datasets generated or analyzed during the study will be available from the corresponding author on request.

CRediT authorship contribution statement

Ting Yang: Writing – original draft, Visualization, Validation, Methodology, Formal analysis, Data curation, Conceptualization. **Hong Wei:** Writing – original draft, Visualization, Validation, Methodology, Formal analysis, Conceptualization. **Jie Chen:** Writing – review & editing, Visualization, Validation, Funding acquisition, Formal analysis, Data curation. **Hanyu Jiang:** Writing – review & editing, Visualization, Validation, Methodology, Formal analysis. **Yidi Chen:** Writing – review & editing, Visualization, Validation, Supervision, Formal analysis, Data curation. **Bin Song:** Supervision, Project administration, Funding acquisition.

Declaration of competing interest

The authors declare that they have no known competing financial interests or personal relationships that could have appeared to influence the work reported in this paper.

Acknowledgement

none.

Acknowledgments

None to declare.

Appendix ASupplementary data

Supplementary data to this article can be found online at https://doi.org/10.1016/j.heliyon.2023.e23448.

References

[1] A.L. Van Dyke, M.S. Shiels, G.S. Jones, et al., Biliary tract cancer incidence and trends in the United States by demographic group, Cancer 125 (9) (2019) 1489–1498, https://doi.org/10.1002/cncr.31942, 1999-2013.
[2] P.J. Brindley, M. Bachini, S.I. Ilyas, et al., Cholangiocarcinoma. Nat Rev Dis Primers. 7 (1) (2021) 65, https://doi.org/10.1038/s41572-021-00300-2. Published 2021 Sep. 9.
[3] D.H. Lee, B. Kim, E.S. Lee, et al., Radiologic evaluation and structured reporting form for extrahepatic bile duct cancer: 2019 consensus recommendations from the Korean society of abdominal radiology, Korean J. Radiol. 22 (1) (2021) 41–62, https://doi.org/10.3348/kjr.2019.0803.
[4] Y. Murakami, K. Uemura, T. Sudo, et al., Prognostic factors after surgical resection for intrahepatic, hilar, and distal cholangiocarcinoma, Ann. Surg Oncol. 18 (3) (2011) 651–658, https://doi.org/10.1245/s10434-010-1325-4.
[5] M. Nagino, S. Hirano, H. Yoshitomi, et al., Clinical practice guidelines for the management of biliary tract cancers 2019: the 3rd English edition, J Hepatobiliary Pancreat Sci 28 (1) (2021) 26–54, https://doi.org/10.1002/jhbp.870.
[6] N.K. Lee, S. Kim, H.I. Seo, D.U. Kim, H.Y. Woo, T.U. Kim, Diffusion-weighted MR imaging for the differentiation of malignant from benign strictures in the periampullary region, Eur. Radiol. 23 (5) (2013) 1288–1296, https://doi.org/10.1007/s00330-012-2725-6.
[7] H.J. Park, S.H. Kim, K.M. Jang, S.Y. Choi, S.J. Lee, D. Choi, The role of diffusion-weighted MR imaging for differentiating benign from malignant bile duct strictures, Eur. Radiol. 24 (4) (2014) 947–958, https://doi.org/10.1007/s00330-014-3097-x.
[8] M.J. Park, Y.K. Kim, S. Lim, H. Rhim, W.J. Lee, Hilar cholangiocarcinoma: value of adding DW imaging to gadoxetic acid-enhanced MR imaging with MR cholangiopancreatography for preoperative evaluation, Radiology 270 (3) (2014) 768–776, https://doi.org/10.1148/radiol.13130009.
[9] I. Joo, J.M. Lee, J.H. Yoon, Imaging diagnosis of intrahepatic and perihilar cholangiocarcinoma: recent advances and challenges, Radiology 288 (1) (2018) 7–13, https://doi.org/10.1148/radiol.2018171187.
[10] R.M. Gore, R.P. Shelhamer, Biliary tract neoplasms: diagnosis and staging, Cancer Imag. (2007), https://doi.org/10.1102/1470-7330.2007.9016, 7 Spec No A (Special issue A):S15-S23. Published 2007 Oct 1.
[11] M.S. Park, T.K. Kim, K.W. Kim, et al., Differentiation of extrahepatic bile duct cholangiocarcinoma from benign stricture: findings at MRCP versus ERCP, Radiology 233 (1) (2004) 234–240, https://doi.org/10.1148/radiol.2331031446.
[12] J.Y. Kim, J.M. Lee, J.K. Han, et al., Contrast-enhanced MRI combined with MR cholangiopancreatography for the evaluation of patients with biliary strictures: differentiation of malignant from benign bile duct strictures, J. Magn. Reson. Imag. 26 (2) (2007) 304–312, https://doi.org/10.1002/jmri.20973.
[13] H. Choi, E.M. Loyer, C. Charnsangavej, Neoplasms of the liver and the bile ducts, Semin. Roentgenol. 39 (3) (2004) 412–427, https://doi.org/10.1016/j.ro.2004.05.002.
[14] Y. Hori, S.T. Chari, Y. Tsuji, et al., Diagnosing biliary strictures: distinguishing IgG4-related sclerosing cholangitis from cholangiocarcinoma and primary sclerosing cholangitis, Mayo Clin Proc Innov Qual Outcomes 5 (3) (2021) 535–541, https://doi.org/10.1016/j.mayocpiqo.2021.03.005. Published 2021 Jun 10.
[15] T. Kamisawa, T. Nakazawa, S. Tazuma, et al., Clinical practice guidelines for IgG4-related sclerosing cholangitis, J Hepatobiliary Pancreat Sci 26 (1) (2019) 9–42, https://doi.org/10.1002/jhbp.596.
[16] V.S. Katabathina, A.K. Dasyam, N. Dasyam, K. Hosseinzadeh, Adult bile duct strictures: role of MR imaging and MR cholangiopancreatography in characterization, Radiographics 34 (3) (2014) 565–586, https://doi.org/10.1148/rg.343125211.
[17] J.Y. Kim, J.M. Lee, J.K. Han, et al., Contrast-enhanced MRI combined with MR cholangiopancreatography for the evaluation of patients with biliary strictures: differentiation of malignant from benign bile duct strictures, J. Magn. Reson. Imag. 26 (2) (2007) 304–312, https://doi.org/10.1002/jmri.20973.
[18] S. Mantripragada, A. Chawla, Cholangiocarcinoma: Part 1, pathological and morphological subtypes, spectrum of imaging appearances, prognostic factors and staging, Curr. Probl. Diagn. Radiol. 51 (3) (2022) 351–361, https://doi.org/10.1067/j.cpradiol.2021.03.008.
[19] WHO Classification of tumors: digestive system tumours, 5th ed.Lyon, France. Available via, https://whobluebooks.iarc.fr/publications/index.php. (Accessed 19 January 2021).
[20] X.Y. Cui, H.W. Chen, Role of diffusion-weighted magnetic resonance imaging in the diagnosis of extrahepatic cholangiocarcinoma, World J. Gastroenterol. 16 (25) (2010) 3196–3201, https://doi.org/10.3748/wjg.v16.i25.3196.
[21] X.Y. Cui, H.W. Chen, S. Cai, et al., Diffusion-weighted MR imaging for detection of extrahepatic cholangiocarcinoma, Eur. J. Radiol. 81 (11) (2012) 2961–2965, https://doi.org/10.1016/j.ejrad.2011.12.040.
[22] I. Hosokawa, K. Hayano, K. Furukawa, et al., Preoperative diagnosis of lymph node metastasis of perihilar cholangiocarcinoma using diffusion-weighted magnetic resonance imaging, Ann. Surg Oncol. 29 (9) (2022) 5502–5510, https://doi.org/10.1245/s10434-022-11931-4.
[23] C. Messina, R. Bignone, A. Bruno, et al., Diffusion-weighted imaging in oncology: an update, Cancers 12 (6) (2020) 1493, https://doi.org/10.3390/cancers12061493. Published 2020 Jun 8.
[24] A.A. Malayeri, R.H. El Khouli, A. Zaheer, et al., Principles and applications of diffusion-weighted imaging in cancer detection, staging, and treatment follow-up, Radiographics 31 (6) (2011) 1773–1791, https://doi.org/10.1148/rg.316115515.
[25] Y. Qiu, J. He, X. Chen, P. Huang, K. Hu, H. Yan, The diagnostic value of five serum tumor markers for patients with cholangiocarcinoma, Clin. Chim. Acta 480 (2018) 186–192, https://doi.org/10.1016/j.cca.2018.02.008.
[26] M. Felder, A. Kapur, J. Gonzalez-Bosquet, et al., MUC16 (CA125): tumor biomarker to cancer therapy, a work in progress, Mol. Cancer 13 (2014) 129, https://doi.org/10.1186/1476-4598-13-129. Published 2014 May 29.

[27] O. Clements, J. Eliahoo, J.U. Kim, S.D. Taylor-Robinson, S.A. Khan, Risk factors for intrahepatic and extrahepatic cholangiocarcinoma: a systematic review and meta-analysis, J. Hepatol. 72 (1) (2020) 95–103, https://doi.org/10.1016/j.jhep.2019.09.007.
[28] B.S. Lee, E.C. Park, S.W. Park, C.M. Nam, J. Roh, Hepatitis B virus infection, diabetes mellitus, and their synergism for cholangiocarcinoma development: a case-control study in Korea, World J. Gastroenterol. 21 (2) (2015) 502–510, https://doi.org/10.3748/wjg.v21.i2.502.
[29] L.Y. Tao, X.D. He, Q. Qu, et al., Risk factors for intrahepatic and extrahepatic cholangiocarcinoma: a case-control study in China, Liver Int. 30 (2) (2010) 215–221, https://doi.org/10.1111/j.1478-3231.2009.02149.x.
[30] J. Toouli, T.A. Wright, Gallstones, Med. J. Aust. 169 (3) (1998) 166–171, https://doi.org/10.5694/j.1326-5377.1998.tb116020.x.
[31] X.Y. Cui, H.W. Chen, S. Cai, et al., Diffusion-weighted MR imaging for detection of extrahepatic cholangiocarcinoma, Eur. J. Radiol. 81 (11) (2012) 2961–2965, https://doi.org/10.1016/j.ejrad.2011.12.040.